# PART 2:

# STRUCTURE
# AND ATMOSPHERES

# Statistical patterns in ground-based transit surveys

**Andrew Collier Cameron**[1]

[1]SUPA, School of Physics & Astronomy, University of St Andrews,
North Haugh, St Andrews KY16 9SS, UK
email: `andrew.cameron@st-andrews.ac.uk`

**Abstract.** As the number of known transiting planets from ground-based surveys passes the 100 mark, it is becoming possible to perform meaningful statistical analyses on their physical properties. Caution is needed in their interpretation, because subtle differences in survey strategy can lead to surprising selection effects affecting the distributions of planetary orbital periods and radii, and of host-star metallicity. Despite these difficulties, the planetary mass-radius relation appears to conform more or less to theoretical expectations in the mass range from Saturns to super-Jupiters. The inflated radii of many hot Jupiters indicate that environmental factors can have a dramatic effect on planetary structure, and may even lead to catastrophic loss of the planetary envelope under extreme irradiation. High-precision radial velocities and secondary-eclipse timing are yielding eccentricity measurements of exquisite precision. They show some hot Jupiters to be in almost perfectly circular orbits, while others remain slightly but significantly eccentric.

**Keywords.** planetary systems, techniques: radial velocities, techniques: photometric

## 1. Introduction

Among the 110 or so transiting planets discovered up to the end of 2010, 79 have been accounted for by five major ground-based wide-field photometric surveys: OGLE-III (Udalski *et al.* 2002), the Transatlantic Exoplanet Survey (TrES; Alonso *et al.* 2004), the Hungarian Automated Transit Network (HATNet; Bakos *et al.* 2004), the Wide-Angle Search for Planets (WASP; Pollacco *et al.* 2006) and the XO Project (McCullough *et al.* 2005). The last four of these employ commercial camera lenses of 11 cm aperture and 200mm focal length, backed by large-format CCD detectors giving fields of view of order 8 degrees square per camera. They achieve differential photometric precisions of order 0.01 magnitude, sufficient to detect transits of Jupiter-sized planets, on stars with $V = 12$. The host stars are thus bright enough that the essential radial-velocity follow-up can be carried out using high-precision radial-velocity spectrometers on telescopes of moderate size. The SOPHIE spectrograph on the 1.9-m telescope at Haute-Provence, the CORALIE spectrometer on the 1.2-m Swiss Euler telescope at La Silla, the FIES spectrograph on the 2.5-m Nordic optical Telescope on La Palma, and the TRES instrument on the 1.5-m Tillinghast reflector telescope on Mount Hopkins have provided the large amounts of radial-velocity followup time needed to eliminate astrophysical false positives and determine planetary masses.

## 2. Survey strategies and system properties

A number of important statistical trends are beginning to emerge from these surveys. Their interpretation must, however, be tempered by an understanding of the systematic

errors inherent in such surveys. For example, Charbonneau (this volume) notes that the distributions of host-star metallicity, planet radius and orbital period differ significantly between the two most prolific surveys, HATNet and WASP.

HATNet operates sites at widely-distributed longitudes, whereas WASP operates from a single site in each hemisphere. This enables HATNet to detect long-period planets with greater efficiency than WASP, whose ability to amass sufficient transits to secure a detection in a single season is hampered by a relatively low day/night duty cycle. WASP employs a raster observing pattern, sweeping the 8 cameras on each mount across 6 or 7 hours in RA with a cadence of about 10 minutes. The very wide area coverage of this strategy enables WASP to detect rare objects with relatively deep transits despite its low cadence and sparse duty cycle. HATNet's more intensive observing strategy and multi-longitude duty cycle is better suited to the detection of shallow transits and hence smaller planets.

A more puzzling difference between the two surveys is that the host stars of the WASP planets have a distribution of metallicities whose median [Fe/H] is close to solar, whereas the HAT planet hosts have a median [Fe/H] that is $\sim 0.2$ dex more metal rich. The HATNet cameras employ Cousins $I$ filters, whereas the WASP cameras use only a red blocking filter with a cutoff at 750 nm. The median $V$ magnitude of the HAT planet-host stars is nearly a magnitude brighter than the WASP median. Experiments with the Besançon galactic model (Robin *et al.* 2003) show that, at the intermediate galactic latitudes where these surveys are conducted, stars of luminosity class V show a steady decrease in median metallicity with increasing $V$ magnitude. Although this trend is not in itself sufficient to explain the difference in the two samples, metal-poor stars of a given $I$ magnitude also appear brighter in the WASP cameras owing to their lower line blanketing. Although further investigation is needed, a combination of these two effects provides a plausible explanation of the difference in metallicity between the HAT and WASP host-star populations.

## 3. Mass-radius relation for transiting planets

The mass-radius relation for transiting planets provides the most basic test of our understanding of their interior structure and composition. The fundamental theory was developed by Zapolsky & Salpeter (1969): at low masses, cold spheres of a given composition follow a mass-radius relation governed by electrostatic forces, yielding densities almost independent of mass such that $R \propto M^{1/3}$. For planets of roughly Neptune mass or less, the spread in the mass-radius relation is effectively a composition sequence, and the density of a planetary body is a fairly reliable guide to its likely composition (Seager *et al.* 2007). At masses comparable to that of Jupiter, the dependence on mass flattens off and eventually turns over to follow a relation of the form $R \propto M^{-1/3}$, in which non-relativistic electron degeneracy pressure is balanced by gravitation. Most of the planets found in ground-based transit surveys (Fig. 1) are in the Jovian mass regime, where radius is more or less independent of mass. The few objects found in the brown-dwarf desert, such as the 60 $M_{\rm Jup}$ WASP-30b, have systematically smaller radii than the Jupiter-mass planets, as do the Saturn-mass and Neptune-mass planets. This pattern is in broad agreement with theoretical expectations. Within each mass range, however, there is a substantial spread in planet radii.

Fressin *et al.* (2007) modelled the radius anomalies of hot Jupiters in terms of their rock/ice core masses and equilibrium temperatures. The equilibrium temperature of a planet is obtained by balancing the irradiating power against re-radiated power assuming a black-body spectrum and re-radiation from a specified fraction of the planetary surface.
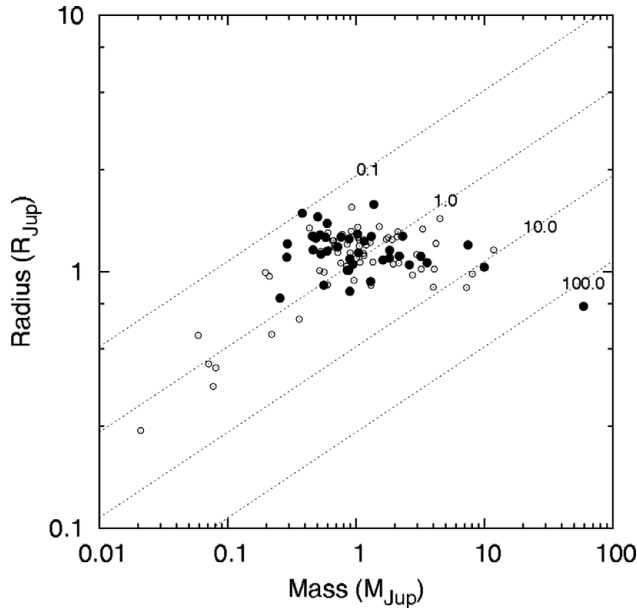
**Figure 1.** Planet radius versus planet mass. Dashed lines denote contours of constant density labelled in Jovian units. Filled symbols denote WASP planets. While there is a substantial spread in radii at each mass, the lower envelope attains its greatest radius at masses close to that of Jupiter.

Fressin *et al.* assumed that 0.5% of the incoming power was dissipated in the planetary core. In these models, the resulting inflation of the planetary radius increases dramatically with decreasing mass. Enoch *et al.* (2010) demonstrated that a strong correlation between planet radius and irradiating flux is indeed present among transiting planets in the mass range between 0.4 and 0.7 $M_{Jup}$.

As Fig. 2 shows, the most inflated gas-giant planets at a given mass tend also to be the most strongly irradiated. There appears to be a sharp upper boundary to the irradiating flux, beyond which no planets are found. The critical irradiating flux at the boundary is mass-dependent, with more massive planets apparently being able to sustain greater irradiating fluxes. Baraffe *et al.* (2004) predicted that the response of a gas-giant planet to mass loss driven by strong irradiation could lead to catastrophic evaporation of the gaseous planetary envelope. The runaway occurs when the evaporation timescale $m/\dot{M}$ becomes significantly shorter than the Kelvin-Helmholtz timescale of the envelope.

## 4. Orbital eccentricities

Among exoplanets in general, high orbital eccentricities tend to be the rule rather than the exception. At the small orbital separations less than about 0.07 AU that favour the discovery of transiting planets, however, low orbital eccentricities are found to be the norm. Planets found in radial-velocity surveys at these small separations also include a significant number of objects with orbital eccentricities indistinguishable from zero.

Among these close-orbiting planets, however, a substantial minority are reported to show significant orbital eccentricities. Some caution must be exercised in interpreting the apparent significance of eccentricities derived from radial-velocity curves. When modelling RV curves it is common practice to use $h = e\cos\omega$ and $k = e\sin\omega$ as fitting parameters, since these two parameters are far less strongly correlated than $e$ and $\omega$
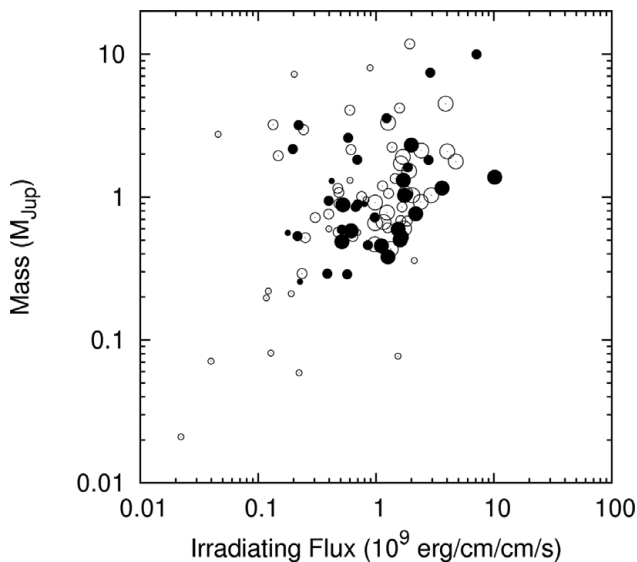
**Figure 2.** Planet mass versus irradiating flux. Large symbols represent planets with radii $R_p > 1.3R_{\rm J}$; medium symbols $1.0R_{\rm J} < R_p < 1.3R_{\rm J}$; small symbols $R_p < 1.0R_{\rm J}$. Filled symbols denote WASP planets. The most inflated gas-giant planets cluster against a sharp upper limit to the irradiating flux, beyond which no gas-giant planets are found at a given mass.

(Ford 2006). As Ford points out in the same paper, however, this convenience carries a price. If the mass of the planet is low, the amplitude $K$ of the stellar reflex orbit may be little greater than the uncertainty on a single RV observation. Even if the reality of the orbit is established beyond question, the eccentricity may be poorly determined. Any asymmetry in the distribution of the RV observations around the orbit can then produce a spurious eccentricity. This effect is seen clearly in the right-hand panel of Fig. 3: both the eccentricity and its uncertainty increase markedly with decreasing radial-velocity amplitude. Ford notes that when the eccentricity is poorly constrained, the use of $h$ and $k$ as fitting parameters in a Markov-chain Monte-Carlo fitting algorithm implicitly imposes a prior on $e$ that is linearly proportional to $e$. This is readily understood by considering the areas of annuli of radius $e$ and width $de$ in $(h, k)$ space where the algorithm is executing a random walk.

Binary-star orbit modelling suffers from the same problem, as was discussed nearly forty years ago by Lucy & Sweeney (1971). They devised a simple $F$-test approach to determining the "false-alarm" probability that the fitted eccentricity would exceed a given value by chance if the true orbit is circular. As a rule of thumb, Lucy & Sweeney calculate that a circular orbit will yield a spurious detection of $2.45\sigma$ or more, with a probability of 5 percent. This is a best-case scenario, assuming the observations to be uniformly distributed in phase. To be on the safe side it is always advisable to examine carefully the improvement in the fit that results from fitting an eccentric as opposed to a circular orbit. Several simple but powerful statistical tools are available to achieve this. The Lucy-Sweeney test and the Bayesian Information Criterion e.g. Liddle 2007) are both effective at determining the true level of significance of an eccentricity detection arising from a given data set, in terms of the number of data points and the improvement in $\chi^2$ produced by the introduction of two additional free parameters in the model.

So which eccentricity determinations is it safe to believe? Among the 30 WASP planets currently listed at exoplanet.eu, only WASP-8b, WASP-14 and HAT-P-14b(=WASP-27b)
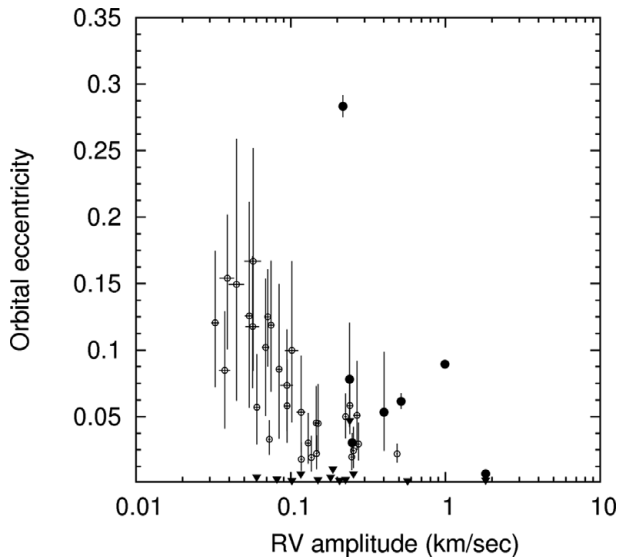
**Figure 3.** Fitted orbital eccentricity versus orbital velocity semi-amplitude $K$. Filled dots denote fits for which the Lucy-Sweeney test yields a probability less than 5% that the improvement in the fit for an eccentric orbit could have arisen by chance from an underlying circular orbit. Filled inverted triangles denote upper limits on $e \cos \omega$ derived from secondary-eclipse timing.

have orbital eccentricities that have a greater than 97% chance of being significantly eccentric on the basis of the original discovery data. Even the massive, close-orbiting WASP-18b (Hellier 2009) has an eccentricity which, despite appearing significant at the 3.3-$\sigma$ level in the discovery data, has a 17% chance of being spurious according to the Lucy-Sweeney test. Subsequent RV observations by Triaud *et al.* (2010), however, reduce the Lucy-Sweeney false-alarm probability to 2.7%, showing WASP-18b to have a small but genuinely significant $e \sin \omega$.

In other cases where eccentricities of marginal significance have been detected, *SPITZER* and ground-based secondary-eclipse mid-times and durations place tight constraints on $e \cos \omega$ and to a lesser extent $e \sin \omega$. Nymeyer *et al.* (2010), for example, find $e \cos \omega = 0.0002 \pm 0.0005$ for WASP-18b. WASP-1b, WASP-2b have $e \cos \omega$ less than 0.003 and 0.004 respectively Wheatley *et al.* (2010). Campo *et al.* (2011) obtain $e \cos \omega = 0.0016 \pm 0.0007$ for WASP-12b, while admitting $e \sin \omega = 0.063 \pm 0.014$ constrained mainly by spectroscopic radial velocities. The Lucy-Sweeney test indicates a 17% chance that this component too could be spurious. Other published secondary-eclipse timings from *SPITZER* reveal insignificant displacements of secondary eclipse from phase 0.5 in HD 209458b (Deming *et al.* 2005), HAT-P-1b (Todorov *et al.* 2010) and TrES-2b (O'Donovan *et al.* 2010), a small but marginally significant displacement in CoRoT-2b (Gillon *et al.* 2010) and a clear confirmation of the orbital eccentricity of GJ436b (Deming *et al.* 2007) .

Orbital eccentricity has the potential to bias our estimates of stellar masses and radii. The total duration, depth and shape of the transit profile determine the planet's radius from the directly-measured stellar density and an estimate of the stellar mass (Seager & Mallén-Ornelas 2003). The estimate of the scaled stellar radius $R_*/a$ scales as $1 + e \sin \omega$ to first order. If transit occurs near periastron, when the planet is travelling fastest, the stellar and planet radii will be underestimated by this factor. The secondary-eclipse timings obtained so far thus suggest that it is generally safer to assume a circular

orbit than to allow a potentially-spurious eccentricity to influence the planetary radius estimate.

## 5. Summary and conclusions

The mass-radius relation for the lowest-mass exoplanets detected from the ground is consistent with a composition sequence. Among the gas-giant planets, the turn-over in radius expected from the physics of cold bodies is becoming apparent, but the relation is broadened significantly by irradiation and the presence of dense rocky cores in some planets. There is a surprisingly sharp boundary in the planet mass - irradiating flux plane, along which the most strongly-inflated planets tend to lie at any given mass. This may indicate that planets undergo catastrophic evaporative mass loss beyond a critical level of irradiation. Secondary-eclipse timing studies of close-orbiting low-mass planets are beginning to provide important insights into the distribution of orbital eccentricities among planets with low radial-velocity amplitudes. The evidence available so far suggests that the orbits of most hot Jupiters have true eccentricities at least an order of magnitude lower than the upper limits obtained from fits to their radial-velocity orbits.

## References

Alonso, R., *et al.* 2004, *ApJ*, 613, L153

Bakos, G., Noyes, R. W., Kovács, G., Stanek, K. Z., Sasselov, D. D., & Domsa, I. 2004, *PASP*, 116, 266

Baraffe, I., Selsis, F., Chabrier, G., Barman, T. S., Allard, F., Hauschildt, P. H., & Lammer, H. 2004, *A&A*, 419, L13

Campo, C. J., *et al.* 2011, *ApJ*, 727, 125

Deming, D., Seager, S., Richardson, L. J., & Harrington, J. 2005, *Nature*, 434, 740

Deming, D., Harrington, J., Laughlin, G., Seager, S., Navarro, S. B., Bowman, W. C., & Horning, K. 2007, *ApJ*, 667, L199

Enoch, B., *et al.* 2011, *MNRAS*, 410, 1631

Ford, E. B. 2006, *ApJ*, 642, 505

Fressin, F., Guillot, T., Morello, V., & Pont, F. 2007, *A&A*, 475, 729

Gillon, M., *et al.* 2010, *A&A*, 511, A3

Hellier, C., *et al.* 2009, *Nature*, 460, 1098

Liddle, A. R. 2007, *MNRAS*, 377, L74

Lucy, L. B. & Sweeney, M. A. 1971, *AJ*, 76, 544

McCullough, P. R., Stys, J. E., Valenti, J. A., Fleming, S. W., Janes, K. A., & Heasley, J. N. 2005, *PASP*, 117, 783

Nymeyer, S., *et al.* 2010, *arXiv:1005.1017*

O'Donovan, F. T., Charbonneau, D., Harrington, J., Madhusudhan, N., Seager, S., Deming, D., & Knutson, H. A. 2010, *ApJ*, 710, 1551

Pollacco, D. L., *et al.* 2006, *PASP*, 118, 1407

Robin, A. C., Reylé, C., Derrière, S., & Picaud, S. 2003, *A&A*, 409, 523

Seager, S. & Mallén-Ornelas, G. 2003, *ApJ*, 585, 1038

Seager, S., Kuchner, M., Hier-Majumder, C. A., & Militzer, B. 2007, *ApJ*, 669, 1279

Todorov, K., Deming, D., Harrington, J., Stevenson, K. B., Bowman, W. C., Nymeyer, S., Fortney, J. J., & Bakos, G. A. 2010, *ApJ*, 708, 498

Triaud, A. H. M. J., *et al.* 2010, *A&A*, 524, A25

Udalski, A., *et al.* 2002, *AcA*, 52, 1

Wheatley, P. J., *et al.* 2010, *arXiv:1004.0836*

Zapolsky, H. S. & Salpeter, E. E. 1969, *ApJ*, 158, 809